

# Benchmark density functional theory calculations for nano-scale conductance.

M. Strange, I. S. Kristensen, and K. S. Thygesen  
*Center for Atomic-scale Materials Design, Department of Physics  
Technical University of Denmark, DK - 2800 Kgs. Lyngby, Denmark*  
(Dated: October 23, 2018)

We present a set of benchmark calculations for the Kohn-Sham elastic transmission function of five representative single-molecule junctions. The transmission functions are calculated using two different density functional theory (DFT) methods, namely an ultrasoft pseudopotential plane wave code in combination with maximally localized Wannier functions, and the norm-conserving pseudopotential code Siesta which applies an atomic orbital basis set. For all systems we find that the Siesta transmission functions converge toward the plane-wave result as the Siesta basis is enlarged. Overall, we find that an atomic basis with double-zeta and polarization is sufficient (and in some cases even necessary) to ensure quantitative agreement with the plane-wave calculation. We observe a systematic down shift of the Siesta transmission functions relative to the plane-wave results. The effect diminishes as the atomic orbital basis is enlarged, however, the convergence can be rather slow.

PACS numbers: 72.10-d,73.40.Cg,73.63.Rt

## I. INTRODUCTION

First-principles calculations of electrical conductance in nano-scale contacts represents a main challenge in computational nanophysics. The interest for this type of calculations began in the mid-nineties where advances in experimental techniques made it possible to contact individual molecules thereby making it possible study the transport of electrons through true nano-scale structures [1, 2]. Apart from the scientific interest, the development of reliable simulation tools for nano-scale quantum transport is relevant in relation to the continued miniaturization of conventional semi-conductor electronics, but also for the introduction of the new generation of molecule based electronics.

It has by now become standard to calculate conductance in nano-scale contacts by employing a combination of non-equilibrium Green's function theory (NEGF) and ground state density functional theory (DFT). The resulting NEGF-DFT formalism provides a numerically efficient way of evaluating the Landauer-Büttiker conductance due to electrons moving in the effective Kohn-Sham (KS) potential without having to calculate the scattering states explicitly. It has been applied extensively to a number of different systems ranging from pure metallic contacts, over organic molecules to carbon nanotubes suspended between metallic electrodes. Overall the approach has been successful in describing qualitative features and trends [3, 4], however, quantitative agreement with experiments has mainly been obtained for strongly coupled systems such as metallic point contacts, monatomic chains, as well as junctions containing small chemisorbed molecules [5, 6, 7].

It is generally accepted that the NEGF-DFT method only provides an approximation to the true conductance - even if the exact exchange-correlation (xc-)functional could be used, and the quality of the result is expected to be strongly system dependent. Moreover, it is not easy

to estimate the effect of using approximate xc-functionals such as the LDA or GGA. We mention here that more sophisticated methods for quantum transport based on configuration interaction, the *GW* method, time-dependent DFT, and the Kubo formula have recently been proposed [8, 9, 10, 11, 12]. However, these schemes are considerably more demanding than the NEGF-DFT and at present they cannot replace NEGF-DFT in practical applications.

Irrespective of the validity of the NEGF-DFT approach and the role played by the approximate functionals, it remains important to establish a general consensus concerning the exact result of a NEGF-DFT calculation for a given xc-functional and specified system geometry, i.e. a benchmark. Although this might seem trivial, the present situation is rather unsatisfactory as different results have been published by different groups for the same or very similar systems (several examples will be given in the text). Perhaps the best example is provided by benzene di-thiolate between gold contacts where the calculated conductance vary with up to a two orders of magnitude for similar geometries [3, 13, 14, 15, 16, 17, 18].

The relatively large variation of the results indicates that the conductance, or more generally the elastic transmission function, is a highly sensitive quantity. Indeed, the implementation of the open boundary conditions defining the scattering problem represents some numerical challenges. Indeed, small errors in the description of the coupling between the finite scattering region and the infinite leads as well as improper *k*-point samplings in supercell approaches, can introduce significant errors in the resulting transmission function.

In this paper we take a first step towards establishing a common reference for NEGF-DFT calculations by performing benchmark calculations for a set of five representative nano-scale contacts. The benchmarking is achieved by comparing the transmission function obtained using two different and independent, albeit simi-

lar, NEGF-DFT methods: In one case the Hamiltonian is obtained from the Siesta DFT program which uses a basis of localized pseudo atomic orbitals (PAOs) together with norm conserving pseudopotentials. The second method applies a basis of maximally localized Wannier functions (WFs) obtained from the Dacapo DFT code which uses plane-waves and ultra soft pseudopotentials. In both cases we use periodic boundary conditions in the directions perpendicular to the transport direction and we apply the PBE xc-functional [19].

The five reference systems we have chosen for our benchmark study are: (i) A monatomic gold chain with a single CO molecule adsorbed. (ii) A 3-atom Pt chain suspended between Pt electrodes. (iii) An H<sub>2</sub> molecule bridging two Pt electrodes. (iv) Benzene-dithiolate (BDT) between Au electrodes, and (v) Bipyridine between Au electrodes. The systems have been chosen according to the criterion that both experimental data as well as previous NEGF-DFT calculations are available in the literature. Furthermore they are representative in the sense that they cover a broad class of systems: homogeneous and heterogeneous, computationally simple (one-dimensional) and more complex, and strongly as well as weakly coupled.

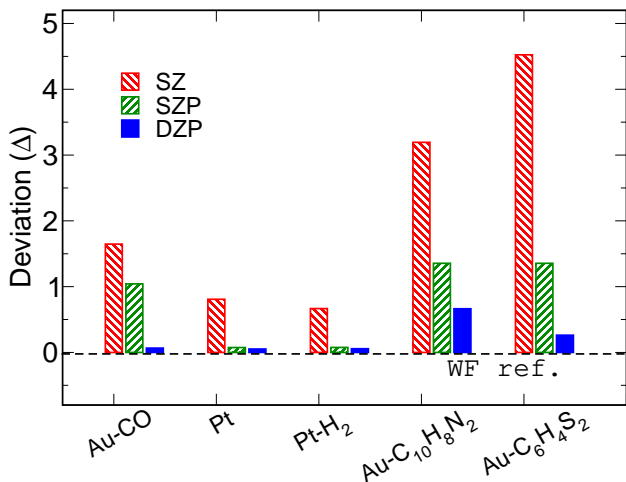


FIG. 1: (color online). Deviation between the WF and Siesta transmission functions for the five reference systems studied. The dashed line indicates zero deviation from the WF transmission. Notice that the Siesta results converge toward the WF result as the PAO basis is enlarged.

A main result of our work is summarized in Fig. 1 where we show the overall deviation

$$\Delta = \int_{-\infty}^{\varepsilon_F + E_0} |T_{\text{WF}}(\varepsilon) - T_{\text{PAO}}(\varepsilon)| d\varepsilon, \quad (1)$$

between the transmission functions calculated using the WF and PAO basis sets, respectively. The cutoff energy  $E_0$  is taken to be the energy above which the WFs are no longer able to reproduce the exact KS eigenstates of the system which is typically  $\sim 3$  eV above the Fermi

level. For all the systems we find that the deviation  $\Delta$  decreases as the Siesta basis is enlarged meaning that the Siesta transmission functions converge toward the WF result. We take this as evidence for the correctness of the WF results and the justification for the use of the term *benchmark* calculation.

In general we find that the double-zeta polarized (DZP) basis provides very good agreement with the WF basis, whereas the single-zeta polarized (SZP) and, in particular, the single-zeta (SZ) basis can produce substantially incorrect features in the transmission function.

The paper is organized as follows. In Sec. II we briefly review the NEGF-DFT formalism and introduce the two specific implementations used in the present study. In Secs. III-VI we present the benchmark calculations for the five reference systems and in Sec. VIII we give our conclusions.

## II. METHOD

In this section we first outline the NEGF-DFT method which has become standard for nanoscale conductance calculations. The two specific NEGF-DFT implementations applied in the present work are then introduced and their key parameters are discussed. We then consider the important issue, common to both methods, of how to treat periodic boundary conditions in the plane perpendicular to the transport direction. We end the section with a discussion of the advantages and disadvantages of the two methods.

### A. NEGF-DFT

The zero temperature, linear response conductance due to non-interacting electrons scattering off a central region ( $C$ ) connected to thermal reservoirs via two ballistic leads ( $L$  and  $R$ ), can be written as

$$G = G_0 T(\varepsilon_F), \quad (2)$$

where  $T(\varepsilon)$  is the elastic transmission function and  $G_0 = 2e^2/h$  is the quantum unit of conductance. Using the NEGF formalism, Meir and Wingreen have derived a very useful formula which expresses the transmission function in terms of the Green's function of the central region [20],

$$T(\varepsilon) = \text{Tr}[G^r(\varepsilon)\Gamma_L(\varepsilon)G^a(\varepsilon)\Gamma_R(\varepsilon)]. \quad (3)$$

In this expression the trace runs over the central region basis functions and  $\Gamma_{L/R}$  is obtained from the lead self-energies (defined in Eq. (5) below) as  $\Gamma_{L/R} = i(\Sigma_{L/R} - \Sigma_{L/R}^\dagger)$ .

In the NEGF-DFT method both the leads and central region are modeled by the effective KS Hamiltonian,  $\hat{h}_{\text{KS}} = -\frac{1}{2}\nabla^2 + v_{\text{eff}}(\mathbf{r})$ . The self-consistent effective potential consists of the well known parts  $v_{\text{eff}} =$

$v_{\text{ext}} + v_H + v_{x_c}$ . Introducing a basis of localized orbitals,  $\{\phi_i\}$ , we define the Hamiltonian and overlap matrices by  $H_{ij} = \langle \phi_i | \hat{h}_{\text{KS}} | \phi_j \rangle$  and  $S_{ij} = \langle \phi_i | \phi_j \rangle$ , respectively. In the original derivation by Meir and Wingreen the basis was assumed orthogonal, but the generalization to non-orthogonal basis sets shows that Eq. (3) still holds when the Green's function is defined as [21]

$$G(z) = [zS_C - H_C - \Sigma_L(z) - \Sigma_R(z)]^{-1}. \quad (4)$$

Here the matrices  $H_C$  and  $S_C$  are the blocks of  $H$  and  $S$  corresponding to the central region basis functions. The retarded Green's function,  $G^r(\varepsilon)$ , is obtained for  $z = \varepsilon + i0^+$ , and the advanced Green's function for  $z = \varepsilon - i0^+$  or  $G^a = (G^r)^\dagger$ .

The self-energy of lead  $\alpha$  is given by

$$\Sigma_\alpha(z) = (zS_{C\alpha} - H_{C\alpha})g_\alpha^0(z)(zS_{\alpha C} - H_{\alpha C}), \quad (5)$$

where  $H_{C\alpha}$  and  $S_{C\alpha}$  are the coupling- and overlap matrix between basis functions in the central region and lead  $\alpha$ , respectively.  $g_\alpha^0$  is the surface Green's function describing the isolated semi-infinite lead,  $g_\alpha^0(z) = [zS_\alpha - H_\alpha]^{-1}$ , which can be calculated recursively using the decimation technique [22].

### B. Method 1: Wannier functions from plane-wave DFT

In method 1 the Kohn-Sham Hamiltonian is obtained from an accurate plane-wave pseudopotential DFT code [23]. The ion cores are replaced by ultrasoft pseudopotentials [24] and we use an energy cutoff of 25 Ry for the plane wave expansion. The Kohn-Sham eigenstates are transformed into partly occupied Wannier functions (WFs) [25] which are used to obtain a tight-binding like representation of the Hamiltonian. The WF's are constructed such that any eigenstate below a selected energy,  $E_0$ , can be exactly represented by a linear combination of WF's. In the applications we have chosen  $E_0$  in the range of 2-4 eV above the Fermi level. In this way the accuracy of the plane-wave calculation is carried over to the WF basis for all energies relevant for transport.

By performing separate DFT calculations for the (periodic) leads and  $C$  we obtain a set of WF's for each region. Note, that  $C$  always contains a few buffer layers of the lead material on both sides of the nano-contact to ensure that the KS potential at the end planes of  $C$  has converged to its value in the leads. Since the WF's in the lead in general will differ from those in the outermost lead unit cells of the central region, care must be taken to evaluate the coupling and overlap matrices  $H_{C\alpha}$  and  $S_{S\alpha}$ . Notice also that although the WF's by construction are orthogonal within each region, WF's belonging to different regions will in general be non-orthogonal. For more details on the construction of the WF's and the calculations of the Hamiltonian matrix for the combined  $L - C - R$  system we refer to Ref. 26. We shall refer to the results obtained from method 1 as the WF results.

### C. Method 2: PAO Siesta basis

Method 2 is based on the DFT code Siesta [27] which uses finite range pseudoatomic orbitals (PAO) [28] as basis functions and Troullier-Martins norm conserving pseudopotentials [29]. As in method 1, the Hamiltonians for the leads and the central region are obtained from separate calculations. Because the KS potential to the left and right of  $C$ , by definition has converged to the value in the leads, we can take the coupling between central region and lead  $\alpha$ ,  $H_{C\alpha}$ , from the pure lead calculation. Note that this is in contrast to method 1, where the different shape of the WF's in the periodic lead and the lead part of the central region makes it essential to evaluate the coupling matrix directly. Note also that this approximation, i.e. the use of the intra-lead coupling matrix elements ( $H_{\alpha\alpha}$ ) in  $H_{C\alpha}$ , can be controlled by including a larger portion of the lead in  $C$ . In practice we find that 3-4 atomic layers must be included in  $C$  on both sides of the junction to obtain converged conductances.

In the present study we restrict ourself to the standard PAOs for Siesta: SZ, SZP and DZP. For the confinement energy, determining the range of PAOs, we use 0.01 Ry and for the meshcutoff we use 200 Ry.

### D. Common ingredients

In both methods 1 and 2 we treat exchange and correlation effects with the PBE energy functional [19]. Furthermore, we impose periodic boundary conditions in the surface plane directions. This means that we are in fact considering the conductance of a periodic array of junctions instead of just a single junction. Instead of the localized basis function  $\phi_n(\mathbf{r})$  (this could be a WF or a PAO) we thus consider the Bloch function

$$\chi_{n\mathbf{k}_\parallel} = \sum_{\mathbf{R}_\parallel} e^{i\mathbf{k}_\parallel \cdot \mathbf{R}_\parallel} \phi_n(\mathbf{r} - \mathbf{R}_\parallel), \quad (6)$$

where  $\mathbf{R}_\parallel$  runs over supercells in the surface plane and  $\mathbf{k}_\parallel$  is a wave-vector in the corresponding two-dimensional Brillouin zone (BZ). Since  $\mathbf{k}_\parallel$  is a good quantum number, we can construct the Hamiltonian,  $H(\mathbf{k}_\parallel)$ , for each  $\mathbf{k}$ -point separately. This in turn implies that the conductance *per* junction is given by the average

$$G = \sum_{\mathbf{k}_\parallel} w(\mathbf{k}_\parallel) G(\mathbf{k}_\parallel), \quad (7)$$

where  $w(\mathbf{k}_\parallel)$  are symmetry determined weight factors. Unless stated otherwise, we have used a  $4 \times 4$  Monkhorst-Pack  $\mathbf{k}_\parallel$ -point sampling of the surface BZ, which for all the systems studied yields conductances converged to within a few percent [26, 30]. We take the Fermi level of the bulk lead as the common Fermi level of the combined system by shifting the levels in the central region by a constant. This is done by adding to  $H_C$  the matrix  $\delta S_c$ ,

where  $\delta = [H_L]_{0,0} - [H_C]_{0,0}$  and the  $(0,0)$  element corresponds to the onsite energy of a basis function located near the interface between  $L$  and  $C$ .

The main advantages of method 1 are: (i) The accuracy of the plane wave calculation carries over to the WF basis set. (ii) The WFs basis set is truly minimal and often results in even fewer basis functions than a SZ basis. The WF basis thus combines high accuracy with high efficiency. The price one has to pay is that the actual construction of well localized WFs is not always straightforward, and requires some user interaction - in particular for metallic systems. Also the lack of finite support of the WFs is unwanted in the context of transport, although in practice it is not a serious problem since the WFs are well localized. Finally, as already explained above, the risk of obtaining different WFs for two similar but non-identical systems renders it less straightforward to patch the parts together using the Hamiltonians obtained for the separate calculations.

Most of the disadvantages of the WF basis are resolved by the PAO basis set: by construction they have finite support and are identical as long as the atomic species on which they are located are the same. This renders it straightforward to patch together Hamiltonians for separate sub systems as long as the KS potential can be smoothly matched at the interfaces. On the other hand, to obtain an accuracy matching the WFs, one needs to use a significantly larger number of orbitals and thus longer computation times as compared to the WF method.

### III. GOLD CHAIN WITH CO

In this section we calculate the conductance of an infinite gold chain with a single CO molecule adsorbed. Scanning tunneling microscope (STM) experiments suggest that CO strongly depresses the transport of electrons through gold wires [31]. This has been supported by NEGF-DFT calculations [32] which shows that the transmission function indeed drops to zero at the Fermi level. The use of infinite gold chains as leads is clearly an oversimplification of the real situation, however, the model seems to capture the essential physics, i.e. the suppression of the conductance, and furthermore is well suited as a benchmark system due to its simplicity.

The geometry of the system is shown in Fig. 2(a). We use a supercell with transverse dimensions  $12\text{\AA} \times 12\text{\AA}$  and take all bond lengths from Ref. 32:  $d_{\text{Au-Au}} = 2.9\text{\AA}$ ,  $d_{\text{Au-C}} = 1.96\text{\AA}$ , and  $d_{\text{C-O}} = 1.15\text{\AA}$ . The Au atom holding the CO is shifted towards CO by  $0.2\text{\AA}$ . In method 1 we obtain six WFs per Au atom and seven WFs for the CO molecular states. Due to the elongated bond length of the Au-wire, we found it necessary in method 2 to increase the range of the Au PAOs in order to converge the band-structure of the Au-wire. The confinement energy was therefore in this case set to  $10^{-4}\text{Ry}$ .

In Fig. 2(b) we show the calculated transmission func-

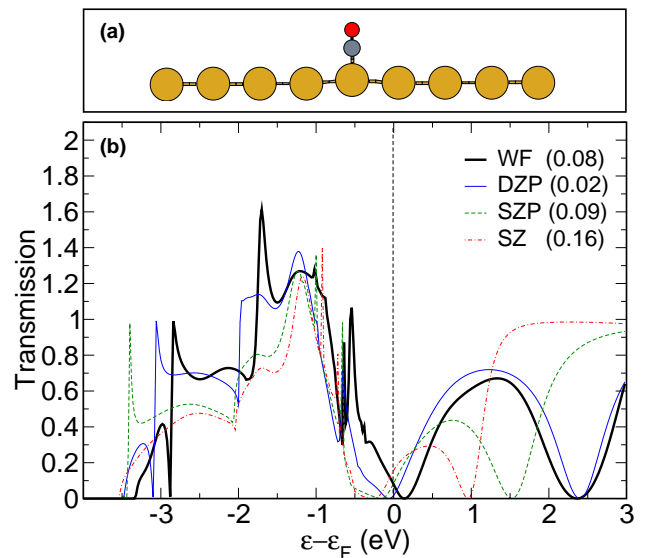


FIG. 2: (color online). (a) Central region used to describe a single CO molecule adsorbed on a monatomic Au wire. (b) Transmission functions for the Au wire CO system calculated using method 1 (WF) and method 2 for three different PAO basis sets. The transmission function at the Fermi level is indicated in the parenthesis following the legends.

tion using three different PAO basis sets and the WF basis set. Overall, the PAO result approaches the WF result as the basis set is enlarged. For the largest PAO basis (DZP) the agreement is in fact very satisfactory given the differences in the underlying DFT methods, e.g. ultrasoft- versus norm-conserving pseudo potentials. The remaining difference can be further reduced by a rigid shift of the DZP transmission by about  $0.15\text{ eV}$ .

All transmission functions feature an anti-resonance near the Fermi level. However, upon enlarging the PAO basis the position of the anti-resonance shifts as follows: (SZ)  $-0.27\text{ eV}$ , (SZP)  $-0.16\text{ eV}$ , (DZP)  $-0.06\text{ eV}$ , and (WF)  $0.12\text{ eV}$ . Note that the position of the anti-resonance obtained with the WFs is approached as the PAO basis set is increased. Also, the curvature of the anti-resonance is improved as the PAO basis set is enlarged. The improvement in these features are, however, not directly reflected in the conductances indicated in the parenthesis following the legends in Fig. 2(b). The reason for this apparent disagreement is the rigid shift between the PAO and WF transmission functions.

We observe that our results differs from the calculation in Ref. 32: While the latter finds two peaks in the energy range  $0-2\text{ eV}$  our converged transmission function shows a single broad peak. In general, both our PAO and WF based transmission functions present less structure than the transmission function reported in Ref. 32. We suspect that these differences are related to the way the coupling  $V_{\alpha C}$  is calculated.

#### IV. PT CONTACT

Atomic point contacts formed from late transition metals such as Au, Pt, and Pd show very stable and reproducible features in conductance measurements [1]. This, together with the simplicity implied by their homogeneity, makes them ideal as benchmark systems for transport calculations. Here we consider the conductance of a pure Pt contact for which both experimental conductance data [33, 34, 35] as well as theoretical calculations [5, 7, 36] are available.

Conductance histograms obtained from mechanically controlled break junction experiments on pure Pt samples show a peak near  $1.5 G_0$ , indicating that as a Pt contact is pulled structures with a conductance around  $1.5 G_0$  are frequently formed. NEGF-DFT calculations have shown that (zig-zag) monatomic Pt chains indeed have a conductance close to this value [5, 7, 35]. Moreover, the calculations predict an increasing conductance as the Pt chain is stretched and evolves from a zig-zag to a linear configuration. This effect has also been observed experimentally [35].

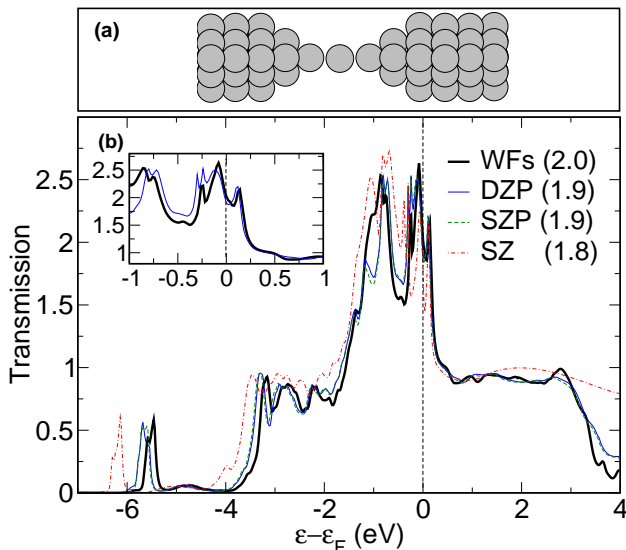


FIG. 3: (color online). (a) Supercell used for the DFT calculation of a short linear Pt chain between Pt(111) surfaces. (b) The calculated transmission function using method 1 and method 2. The transmission at the Fermi level is indicated in the parenthesis following the legends. In the inset we show the transmission function in the important region near the Fermi level for the DZP basis set and the WF basis set.

In Fig. 3(a) we show the supercell used to model the scattering region of the Pt contact. The Pt contact is modeled by two four-atom pyramids attached to (111) surfaces containing  $3 \times 3$  atoms in the surface plane. In order to ensure that the effective KS potential has converged to its bulk value at the end planes of the supercell we include 3-4 atomic layers (ABC-CABC stacking) on either side of the pyramids. The chain is formed by inserting a single Pt atom between the apex atoms of the

two pyramids. We have relaxed the contact region (pyramids+chain) while keeping the rest of the structure fixed in the bulk configuration with lattice constant  $3.93 \text{ \AA}$  and a distance of  $14.60 \text{ \AA}$  between the (111) surfaces. The cutoff energy used in the construction of WFs was set to  $\varepsilon_F + 4.0 \text{ eV}$  ensuring that the KS eigenstates below this value are exactly reproducible in terms of the WFs.

In Fig. 3(b) we show the calculated transmission functions using method 1 and method 2. The qualitative agreement between the two methods is striking, however, only the SZP and DZP basis sets provide quantitative agreement with the WF result. The SZ basis set results in a down shift of the peak at  $-6 \text{ eV}$  and an incorrect description of the features in the important region near the Fermi level. Here the converged transmission function shows two peaks positioned at  $\varepsilon_F - 0.8 \text{ eV}$  and just below the Fermi level, respectively. The main peak astride the Fermi level in fact consists of three smaller peaks, as seen more clearly in the inset for the DZP and WF basis set. These particular features in the transmission function were also observed in Ref. 36 for a similar Pt contact, employing a method based on quantum chemistry software and a description of the bulk electrodes by a semi empirical tight-binding Hamiltonian on a Bethe lattice [37]. Also, the calculated conductance of  $2.3 G_0$  is in agreement with our results, considering the structural differences.

In Fig. 4 we show the calculated conductance of the Pt contact for three electrode displacements:  $13.62 \text{ \AA}$ ,  $14.60 \text{ \AA}$ , and  $14.75 \text{ \AA}$ . The three configurations correspond to an unstrained Pt chain, the chain just before it snaps, and the broken chain, respectively.

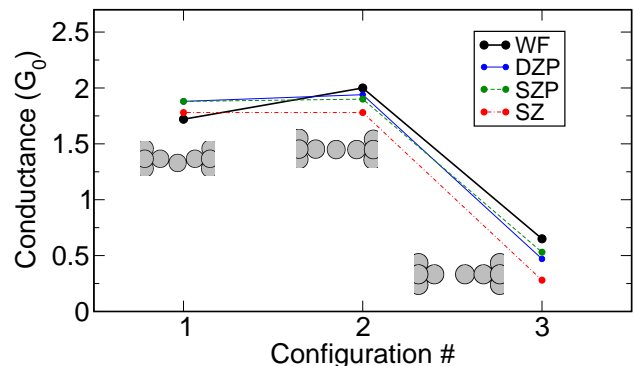


FIG. 4: (color online). Conductance for three different configurations during the stretching of a small Pt chain. Configurations 1, 2, and 3 correspond to the unstrained chain, maximally strained chain, and a broken chain, respectively. The contact atoms are shown in the insets

All basis sets, except for the SZ, are able to reproduce the trend of increasing conductance prior to rupture. The SZ basis set underestimates the absolute conductance by nearly  $0.5 G_0$  in the strained and broken configurations as compared to the WF result. The conductance calculated with the SZP and DZP basis set is almost identical and shows results more consistent with the WF basis for all

three configurations.

## V. PT-H<sub>2</sub>-PT CONTACT

In this section we consider the simplest possible molecular junctions, namely a single hydrogen molecule between metallic Pt contacts. Like the metallic point contacts, the Pt-H<sub>2</sub>-Pt junction shows stable and reproducible behavior in conductance measurements. In particular, a very pronounced peak close to  $1G_0$  appears in the conductance histogram obtained when a Pt contact is broken in a hydrogen atmosphere [33]. Although reported conductance calculations show significant variation (see below), there have been given substantial evidence that the structure responsible for the peak consists of a single hydrogen molecule bridging the Pt contacts [33, 38].

Several groups have published NEGF-DFT calculations for the transmission function of the Pt-H<sub>2</sub>-Pt system. Most find a conductance of  $(0.9 - 1.0)G_0$ , but also much lower values of  $(0.2 - 0.5)G_0$  have been reported. [4, 6, 33, 39, 40].

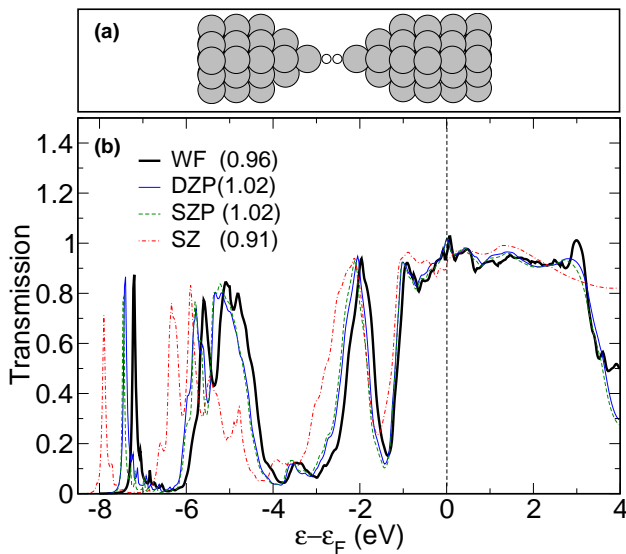


FIG. 5: (color online). (a) Supercell used to model the central region of the Pt-H<sub>2</sub>-Pt junction. (b) Transmission function for the Pt Hydrogen bridge. The transmission function at the Fermi level is indicated in the parenthesis following the legends.

For the benchmark calculations we use the same setup as in Sec. IV with the central Pt atom replaced by a hydrogen molecule, see Fig. 5(a). The relevant bond length determining the structure after relaxation of the Pt pyramids and the hydrogen atoms are  $d_{\text{Pt-H}} = 1.7 \text{ \AA}$  and  $d_{\text{H-H}} = 1.0 \text{ \AA}$ .

In Fig. 5(b) we show the calculated transmission functions. Like in the case of the Pt contact, the agreement between the different calculations is striking, especially

in the important region around the Fermi level. The SZ basis set reproduces the qualitative features of the larger basis sets, but introduces a considerable down shift of the low-lying peaks.

The very good agreement between the two methods indicates that the transmission function for this system is rather insensitive to the basis set. We stress, however, that a proper  $\mathbf{k}_{\parallel}$ -point sampling of the transmission function is crucial to obtain meaningful results independently of the quality of the basis set. Restricting the calculation to the  $\Gamma$  point yields a transmission function with a (unphysical) peak at the Fermi level [6]. We note in passing that such a peak is present in the transmission function reported in Ref. 4. Such unphysical features resulting from an insufficient  $\mathbf{k}_{\parallel}$ -point sampling are not properties of the molecular junction, but are rather due to van Hove singularities in the quasi one-dimensional leads [30]. The results reported in Ref. 40 are based on Siesta DFT code and show good agreement with our results. The conductance obtained in one of the early theoretical calculations [39] on the hydrogen molecular bridge are considerably lower than our and most other results. The calculational method applied in Ref. 39 is, however, the same as applied in the study of pure Pt contacts [36], which agrees well with our results as discussed in Sec. IV. We speculate if this could be related to the smaller size of the Pt cluster used to model the electrodes in 39 as compared to 36. Another possibility for the discrepancies is the use of the B3LYP energy functional in 39 instead of an LDA/GGA functional used in most other works.

## VI. BENZENE-1,4-DITHIOL (BDT) BETWEEN AU(111) SURFACES

The Benzene-1,4-dithiol (BDT) molecule suspended between gold electrodes was among the first single-molecule junctions to be studied and has become the standard reference for calculations of nano-scale conductance. Depending on the experimental setup, measured conductances vary between  $10^{-4} G_0$  and  $10^{-1} G_0$  [41, 42, 43, 44, 45], while the calculated values typically lie in the range  $(0.05 - 0.4) G_0$  [3, 13, 16, 17, 18, 46, 47, 48]. In general it has been found that the transmission function is strongly dependent on the bonding site of the S atom [18, 47], while variations in the Au-S bond length only affects the transmission function weakly [46].

As our objective is to establish a computational benchmark for the Au-BDT system we choose the simple junction geometry shown in Fig. 6(a). The S atoms are placed in fcc hollow sites of the Au(111) surface and the molecule has been relaxed while keeping the Au atoms fixed in the bulk crystal structure. We use an Au lattice constant of  $4.18 \text{ \AA}$ , and a distance between the Au(111) surfaces of  $9.68 \text{ \AA}$ . With these constraints the relevant bond lengths are:  $d_{\text{Au-S}} = 2.45 \text{ \AA}$ ,  $d_{\text{S-C}} = 1.73 \text{ \AA}$ , and  $d_{\text{C-H}} = 1.09 \text{ \AA}$ .

In Fig. 6(b) we show the calculated transmission func-

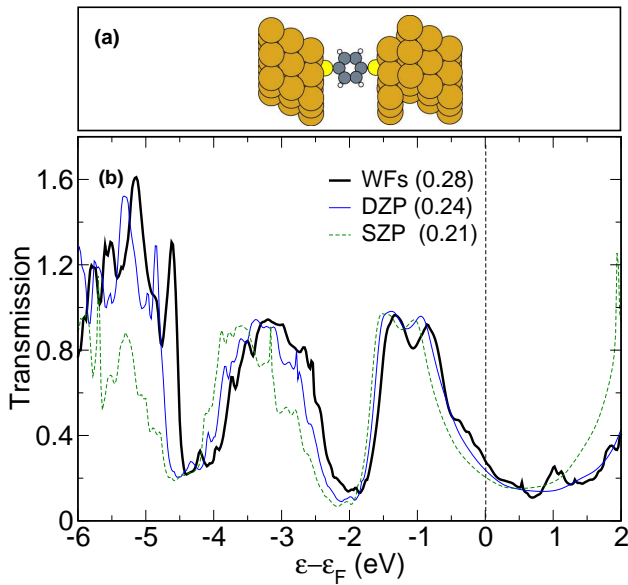


FIG. 6: (color online). (a) Supercell used to model the central region of the Au(111)-BDT-Au(111) system with S at the fcc hollow site. (b) The calculated transmission functions. Note, that the SZ transmission function has been omitted for clarity. The transmission function at the Fermi level is indicated in the parenthesis following the legends.

tions (the SZ result has been omitted for clarity). Notice that we plot the transmission function only up to 2 eV above the Fermi level. This is because the the WF transmission at larger energies is sensitive to the parameters used in the construction of the WFs, in particular the cutoff energy  $E_0$ , and thus we cannot be sure about the WF result above  $2 \text{ eV} + \epsilon_F$ .

The three transmission functions agree very well in the energy range from 2 eV below the Fermi level to 1 eV above the Fermi level, while only the DZP result agrees quantitatively with the WF result in the entire energy range. We again notice the down shift of the PAO transmission functions relative to the WF result.

The presence of a broad transmission peak positioned  $\sim 1 \text{ eV}$  below the Fermi level is in qualitative agreement with previous results [3, 16, 46, 47, 49, 50]. For more stretched configurations, i.e. for larger values of the S-C bond length, than the one used in the present study, the broad peak splits into two more narrow peaks [26].

The transmission function presented in Ref. 3 was obtained using a method very similar to our method 2, however, the reported conductance of  $0.4 G_0$  is almost twice as high as our DZP results of  $0.24 G_0$ . The large conductance arises because the transmission peak closest to the Fermi level is considerably broader than what we find. If, however, we restrict the  $\mathbf{k}_{\parallel}$  to the  $\Gamma$ -point we find the same broadening as in Ref. 3 and a very similar conductance of  $0.37 G_0$ . Another feature of the  $\Gamma$ -point only transmission function is that the second peak positioned at  $\sim 3 \text{ eV}$  below the Fermi level separates into a number of more narrow peaks.

In Ref. 16 the transmission function is calculated from the LMTO-ASA method and averaged over 36 irreducible  $\mathbf{k}_{\parallel}$ -points. Both the width and the position of the two peaks in the transmission function at 1 eV and 3 eV below the Fermi level, are in good agreement with our results. The height of the former peak is, however, lower than in our calculation and this reduces the conductance to a value of  $0.07 G_0$ . We suspect that this difference could be due to differences in the adopted contact geometries.

## VII. BIPYRIDINE BETWEEN AU(111) SURFACES

As the last reference system we consider a bipyridine molecule attached between two gold-electrodes. STM experiments on bipyridine molecules in a toluene solution [51] show that the conductance of Au-bipyridine junctions is quantized in multiples of  $0.01 G_0$  which was interpreted as the formation of stable contacts containing one or more molecules. The conductance is expected to be sensitive to the details of the contact geometry [52], however, for the benchmark calculation we choose the simple case of binding at the on-top site of a flat Au(111) surface, as shown in Fig. 7(a). The Au electrodes are the same as used for the BDT molecule in Sec. VI, the Au(111)-N distance is  $2.180 \text{ \AA}$ , while the electrode displacement is  $11.53 \text{ \AA}$ .

The transmission functions calculated using either PAOs or WFs are shown in Fig. 7(b). At first it is noted that the overall structures of the transmission functions are very similar. In the Siesta calculations, the position of the narrow LUMO peak which governs the transport is underestimated but converges towards the WF result as the PAO basis set is enlarged, see the inset of Fig. 7(b). The alignment of the LUMO energy level with respect to the Fermi level and its relation to charge transfer was studied in Ref. 53.

Several groups have investigated the transport properties of bipyridine-gold junctions, and there is general agreement that the low bias conductance depends crucially on the details of the contact geometry. As different groups have chosen different geometries and models for the gold electrodes a direct comparison of the reported transmission functions is difficult.

To the best of our knowledge the first theoretical paper on the bipyridine system is by Tada *et al.* [54]. In their calculations bipyridine is adsorbed on-top of an Au-atom of a rather small Au cluster, and the coupling to the infinite electrodes is modeled by a broadening parameter fitted to experimental data. The zero-voltage transmission function contains some of the same peak structures as we observe. Hou *et al.* [55] have published several papers on the gold-bipyridine junction. Like Tada *et al.* they include only a few gold atoms in the *ab-initio* calculation and treat the coupling to electrodes through a model self-energy term. The peak structure of the transmission function is quite different from ours. This could be due

to the small size of the gold clusters used to mimick the electrodes. While most other groups observe tunneling through the LUMO tail [52, 53, 56], Hou *et al.* argue that the transport is mainly taking place via the HOMO-2 state. Calculations by Wu *et al.* [57, 58] obtained using a Siesta-based transport code [59], for bipyridine attached to the on-top site of a gold surface show overall good agreement with our results (see Fig. 7(a) in paper 57). The minor differences are probably related to the fact that only the  $\Gamma$ -point has been used in the latter paper.

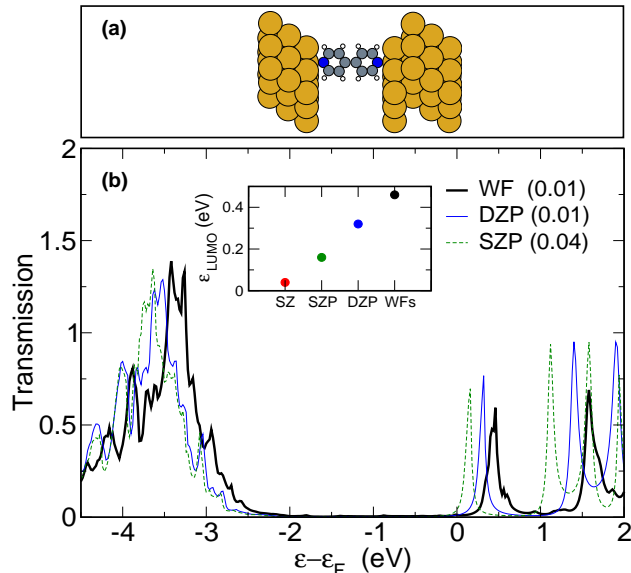


FIG. 7: (color online). (a) Supercell used to describe the central region of the bipyridine-Au(111) junction. (b) Calculated transmission functions (the SZ result has been omitted for clarity). The inset shows the dependence of the LUMO position on the basis sets. The transmission function at the Fermi level is indicated in the parenthesis following the legends.

## VIII. CONCLUSIONS

We have established a set of benchmark calculations for the Kohn-Sham(PBE) elastic transmission function of five representative single-molecule junctions using two different methods based on independent DFT codes: (i) A plane wave DFT code in combination with maximally localized Wannier functions. (ii) The Siesta program which applies finite range pseudoatomic orbitals.

For all five systems we find that the Siesta result converges towards the WF result as the Siesta basis is enlarged from SZ to DZP with the latter yielding very good quantitative agreement with the WF transmission. In the Siesta calculations the transmission peaks relative to the peaks obtained with the plane-wave calculation are systematically shifted toward lower energies. The problem can be overcome by enlarging the Siesta basis, however, the convergence can be rather slow.

## IX. ACKNOWLEDGMENTS

The authors acknowledge support from the Danish Center for Scientific Computing through grant HDW-1103-06. The Center for Atomic-scale Materials Design is sponsored by the Lundbeck Foundation.

- 
- [1] N. Agrait, A. L. Yeyati, and J. M. van Ruitenbeek, *Phys. Rep.* **377**, 81 (2003), and references therein.
- [2] A. Nitzan and M. A. Ratner, *Science* **300**, 1384 (2003).
- [3] K. Stokbro, J. Taylor, M. Brandbyge, J.-L. Mozos, and P. Ordejón, *Comp. Matt. Science* **27**, 151 (2003).
- [4] J. C. Cuevas, J. Heurich, F. Pauly, W. Wenzel, and G. Schön, *Nanotechnology* **14**, R29 (2003).
- [5] V. M. García-Suárez, A. R. Rocha, S.W. Bailey, C. J. Lambert, S. Sanvito, and J. Ferrer, *Phys. Rev. Lett.* **95**, 256804 (2005).
- [6] K. S. Thygesen and K. W. Jacobsen, *Phys. Rev. Lett.* **94**, 036807 (2005).
- [7] M. Strange, K. S. Thygesen, and K. W. Jacobsen, *Phys. Rev. B* **73**, 125424 (2006)
- [8] P. Delaney and J. C. Greer, *Phys. Rev. Lett.* **93**, 036805 (2004).
- [9] K. S. Thygesen and A. Rubio, *J. Chem. Phys.* **126**, 091101 (2007).
- [10] P. Darancet, A. Ferretti, D. Mayou, and V. Olevano, *Phys. Rev. B* **75**, 075102 (2007).
- [11] S. Kurth, G. Stefanucci, C.-O. Almbladh, A. Rubio, and E. K. Gross, *Phys. Rev. B* **72**, 035308 (2005).
- [12] P. Bokes and R. W. Godby, *Phys. Rev. B* **69**, 245420 (2004).
- [13] M. Di Ventura, S. T. Pantelides, and N. D. Lang, *Phys. Rev. Lett.* **84**, 979 (2000)
- [14] D. Q. Andrews, R. Cohen, R. P. Van Duyne, and M. A. Ratner, *J. Chem. Phys.* **125**, 174718 (2006)
- [15] C. Toher and S. Sanvito, *Phys. Rev. Lett.* **98**, 056801 (2007)
- [16] S. V. Faleev, F. Léonard, D. A. Stewart, and M. van Schilfgaarde, *Phys. Rev. B* **71**, 195422 (2005).
- [17] K. Varga and S. T. Pantelides, *Phys. Rev. Lett.* **98**, 076804 (2007).
- [18] J. Tomfohr and O. F. Sankey, *J. Chem. Phys.* **120**, 1542 (2004).
- [19] P. Perdew, K. Burke, and M. Ernzerhof, *Phys. Rev. Lett.* **77** 3865-3868 (1996).
- [20] Y. Meir and N. S. Wingreen, *Phys. Rev. Lett.* **65**, 2512 (1992).
- [21] K. S. Thygesen, *Phys. Rev. B* **73**, 035309 (2006).
- [22] F. Guinea, C. Tejedor, F. Flores, and E. Louis, *Phys. Rev. B*, **28**, 4397 (1983).
- [23] B. Hammer, L.B. Hansen, and J.K. Nørskov, *Phys. Rev. B* **59**, 7413 (1999); S.R. Bahn and K.W. Jacobsen, *Comp. Sci. Eng.* **4**, 56 (2002); The Dacapo code can be downloaded at <http://www.camp.dtu.dk/software>.
- [24] D. Vanderbilt, *Phys. Rev. B* **41**, 7892 (1990).
- [25] K. S. Thygesen, L. B. Hansen, and K. W. Jacobsen, *Phys. Rev. Lett.* **94**, 026405 (2005); K. S. Thygesen, L. B. Hansen, and K. W. Jacobsen, *Phys. Rev. B* **72**, 125119 (2005).
- [26] K. S. Thygesen, and K. W. Jacobsen, *Chemical Physics* **319**, 111-125 (2005)
- [27] J. M. Soler, E. Artacho, J. D. Gale, A. García, J. Junquera, P. Ordejón and D. Sanchez-Portal, *J. Phys. Cond. Matter* **14**, 2745-2779 (2002).
- [28] E. Artacho, D. Sánchez-Portal, P. Ordejón, A. García, J. M. Soler, *Phys. Status Solidi B* **215**, 809 (1999)
- [29] N. Troullier and J. L. Martins, *Solid State Commun.* **74**, 613 (1990)
- [30] K. S. Thygesen and K. W. Jacobsen, *Phys. Rev. B* **72**, 033401 (2005).
- [31] N. Nilius, T.M.Wallis, and W. Ho, *Phys. Rev. Lett.* **90**, 186102 (2003)
- [32] A. Calzolari, C. Cavazzoni, and M. B. Nardelli, *Phys. Rev. Lett.* **93**, 096404 (2004).
- [33] R. H. M Smit, Y. Noat, C. Untiedt, N. D. Lang, M. C. van Hemert, and J. M. van Ruitenbeek, *Nature (London)* **419**, 906 (2002)
- [34] C. Untiedt, D. M. Dekker, D. Djukic, and J. M. van Ruitenbeek, *Phys. Rev. B* **69**, 081401 (2004).
- [35] S. K. Nielsen, Y. Noat, M. Brandbyge, R. H. M. Smit, K. Hansen, L. Y. Chen, A. I. Yanson, F. Besenbacher, and J. M. van Ruitenbeek, *Phys. Rev. B* **67**, 245411 (2003).
- [36] J. Fernández-Rossier, D. Jacob, C. Untiedt, and J. J. Palacios, *Phys. Rev. B* **72**, 224418 (2005).
- [37] J. J. Palacios, A. J. Perez-Jimenez, E. Louis, and J. A. Verges, *Phys. Rev. B* **64**, 115411 (2001).
- [38] D. Djukic, K. S. Thygesen, C. Untiedt, R. H. M. Smit, K. W. Jacobsen, and J. M. van Ruitenbeek, *Phys. Rev. B* **71**, R161402 (2005).
- [39] Y. García,<sup>1</sup> J. J. Palacios, E. SanFabián, J. A. Vergés, A. J. Pérez-Jiménez,<sup>3</sup> and E. Louis, *Phys. Rev. B* **69**, R041402 (2004).
- [40] V. M. García-Suárez,<sup>1</sup> A. R. Rocha, S. W. Bailey, C. J. Lambert, S. Sanvito, and J. Ferrer, *Phys. Rev. B* **72**, 045437 (2005)
- [41] M. A. Reed, C. Zhou, C. J. Muller, T. P. Burgin, and J. M. Tour, *Science* **278**, 252 (1997).
- [42] M. Tsutsui, Y. Teramae, S. Kurokawa, and A. Sakai, *Appl. Phys. Lett.* **89**, 163111 (2006).
- [43] X. Xiao, B. Xu, and N. J. Tao, *Nano Lett.* **4**, 267 (2004).
- [44] J. Ulrich, D. Esrail, W. Pontius, L. Venkataraman, D. Millar, and L. H. Doerrer, *J. Phys. Chem. B* **110**, 2462 (2006).
- [45] S. Ghosh, H. Halimun, A. K. Mahapatro, J. Choi, S. Lodha, and D. Janes, *Appl. Phys. Lett.* **87**, 233509 (2005).
- [46] F. Evers, F. Weigend, and M. Koentopp, *Phys. Rev. B* **69**, 235411 (2004).
- [47] H. Kondo, H. Kino, J. Nara, T. Ozaki, and T. Ohno, *Phys. Rev. B* **73**, 235323 (2006).
- [48] E. G. Emberly and G. Kirczenow, *Phys. Rev. Lett.* **91**, 188301 (2003).
- [49] S.-H. Ke, H.U. Baranger and W. Yang, *cond-mat/0705.3409* (2007).
- [50] Y. Xue, S. Datta, and M. A. Ratner, *J. Chem. Phys.* **115**, 4292 (2001).
- [51] B. Xu and N.J. Tao, *Science* **301**, 1221 (2003).
- [52] R. Stadler, K.S. Thygesen and K.W. Jacobsen, *Phys. Rev. B* **72**, R241401 (2005)
- [53] R. Stadler and K.W. Jacobsen, *Phys. Rev. B* **74**, 161405 (2006).
- [54] T. Tada, M. Kondo and K. Yoshizawa, *J. Chem. Phys.* **121**, 8050 (2004).
- [55] S. Hou, J. Zhang, R. Li, J. Ning, R. Han, Z. Shen, X. Zhao, Z. Xue and Q. Wu, *Nanotechnology* **16**, 239 (2005); S. Hou, J. Ning, Z. Shen X. Zhao and Z. Xue, *Chem. Phys.* **327**, 1 (2006); R. Li, S. Hou, J. Zhang, Z. Qian, Z. Shen and X. Zhao, *J. Chem. Phys.* **125**, 194113 (2006).
- [56] A.J. Perez-Jimenez, *J. Phys. Chem. B* **109**, 10052 (2005).

- [57] X. Wu, Q. Li, J. Huang and J. Yang, *J. Chem. Phys.* **123**, 184712 (2005)
- [58] Q. Li, X. Wu, J. Huang and J. Yang, *Ultramicroscopy* **105**, 293 (2005).
- [59] M. Brandbyge, J.L. Mozos, P. Ordejón, and K. Stokbro, *Phys. Rev. B* **65**, 165401 (2002).